Design and synthesis of new Zn(II) nalidixic acid-DACH based Topo-II inhibiting molecular entity: Chemotherapeutic potential validated by its in vitro binding profile, pBR322 cleavage activity and molecular docking studies with and molecular targets

Farukh Arjmand, Imtiyaz Yousuf, Mohd. Afzal, Loic Toupet

Design and synthesis of new Zn(II) nalidixic acid–DACH based Topo–II inhibiting molecular entity: Chemotherapeutic potential validated by its *in vitro* binding profile, pBR322 cleavage activity and molecular docking studies with DNA and RNA molecular targets.

Farukh Arjmand*[,a], Imtiyaz Yousuf[a], Mohd. Afzal[a], and Loic Toupet[b]

[a]*Department of Chemistry, Aligarh Muslim University, Aligarh 202002, Uttar Pradesh, India*

[b]*Institut de Physique de Rennes, UMR 625, Université de Rennes 1, Campus de Beaulieu Bat. 11 A, 263 av. Général Leclerc, 35042 Rennes Cedex, France.*

*Corresponding author. Tel.: +91 5712703893.

E–mail address: farukh_arjmand@yahoo.co.in (F. Arjmand).

Abstract

Nalidixic acid–DACH based Zn(II) molecular entity (**1**) was synthesized and thoroughly characterized by spectroscopic techniques (FT–IR, ^{1}H and ^{13}C NMR, ESI–MS) and single crystal X–ray crystallography as a potential chemotherapeutic drug candidate. The comparative *in vitro* binding studies of complex **1** with targets like CT–DNA and yeast tRNA were carried out by employing UV–vis, emission spectroscopy, circular dichorism and viscosity which revealed higher binding affinity of **1** towards yeast tRNA as compared to CT–DNA. Complex **1** cleaves pBR322 plasmid *via* hydrolytic pathway (validated by T4 religation assay); in addition, **1** also exhibited significant inhibitory effects on the catalytic activity of Topo–II at a concentration of 30 μM. Further, validation of the interaction studies was accompolished by carrying out molecular docking studies with DNA, RNA and Topo–II targets. This work also advances our knowledge for the development and design of small RNA targeted therapeutic molecules which were relatively under exploited drug targets.

Key words: Nalidixic acid, pBR322 plasmid DNA, T4 DNA ligase enzyme, Molecular docking.

1. Introduction

Interaction of small molecules with nucleic acids has gained prominence over a last few decades owing to their possible applications as nucleic acid structural probes [1–2], artificial nucleases [3–5], therapeutic agents for drug design [6–8]. Nucleic acids, particularly DNA and RNA are prime targets for most of the drugs in the areas of infectious diseases [9,10] *viz.*, HIV, AIDS, hepatitis C and cancer [11]. Interaction of small molecules with DNA causes DNA damage in cancer cells by distorting its structure and inhibits the growth of cancer cells; resulting in cell death or apoptosis [12]. There has been a tremendous drive for the search of sequence–selective DNA binding agents which can be commercialized as cancer chemotherapeutic drugs [13,14]. Various small molecules or compounds which have been isolated and characterized exhibit some disadvantages which limit their application or efficacy as anticancer drugs (Table 1) [15–21].

In an attempt to redeem the modalities for efficient chemotherapeutic agents, presently there is a lot of focus on new RNA–binding molecules for drug design. The interactions between RNA and biological macromolecules are essential for many vital processes in molecular biology *in vivo viz.,* transcription and translation, catalyzing protein syntheses and controls gene expression [22]. Many of these functions actually increase the potential RNA targets for small molecule chemical genetics probes or therapeutics [23]. RNA is chemically similar to DNA and less complex than protein. Despite their chemical similarity (four nucleobases are transcribed in both), there are more examples of small molecules which actually bind DNA *via* non–covalent interactions *viz.*, base stacking (intercalation) [24], electrostatic (phosphate binding) [25] and groove binding [26]. RNA offers several advantages over DNA as a therapeutic agent; i) chromosomal DNA is packed extensively, significantly limiting its accessibility to small molecules while RNA is highly structured ii) DNA repair systems are available in the cell whereas RNA analogous enzymes are virtually unknown iii) RNA

exhibits a high diversity in terms of folding and therefore will have a greater potential for selective targeting based on structure rather than sequence [27].

Inorganic metal complexes have an advantage due their relative ease of synthesis and ability to alter the ligands or metal properties [28], RNA recognition properties [29] and applicability of the complex [30]. Metal–based small therapeutic agents that are more suited for RNA binding abilities are usually coordinatively saturated, inert to substitution, rigid and well defined in structure, since they do not make direct coordination to RNA. These complexes typically bind by non–covalent interactions such as electrostatic, hydrogen bonding, van der Waals interaction, etc. [31]. In addition, these complexes have ability to induce RNA scission by a number of mechanistic pathways that mark their preferential sites [27].

Nalidixic acid belongs to the quinolone family–a major class of synthetic antibacterial agents which is targeted to DNA topoisomerases and DNA gyrase. DNA gyrase is unique in catalysing the negative supercoiling of DNA and is essential for DNA replication, transcription and recombination. Nalidixic acid was shown to bind preferentially to single–stranded rather than double–stranded DNA, thereby provides a rationale for our RNA binding studies [32].

In order to modulate the deleterious effects of antitumor chemotherapeutic drugs, we have combined the structural artefacts; nalidixic acid pharmacophore and 1*R*,2*R*–diaminocyclohexane (DACH) ligand scaffolds with Zn(II) core in **1.** This design bears novelty as the alkyl or aryl groups of nalidixic acid and alicyclic ring of 1*R*,2*R*–diaminocyclohexane moiety are known to increase lipid solubility of polar compounds, thereby facilitating the its delivery through cell membranes (Fig. **1**) therefore it is a suitable carrier ligand which has been effectively utilized in modulation of new therapeutic chemical entities. Zinc, an endogenously biocompatible metal ion is redox inert exists as a divalent cation in the biological system and is actively involved in DNA synthesis,

apoptosis, gene expression, and catalytic functions [33]. Zinc–based nalidixic acid drug candidate **1** is capable of showing DNA/RNA recognition and can efficiently cleave DNA by hydrolytic mechanism that can eventually leads to different cell death mechanism as compared to cisplatin [34].

In the light of our increasing interest in RNA targeted chemotherapeutics, we have carried out the comparative *in vitro* RNA and DNA binding studies, gel electrophoresis and molecular docking studies with **1**; in addition Topo II inhibition assay was also carried out which revealed its outstanding candidature to act as Topo II inhibitor. Drugs like anthracyclines, acridines, ellipticines, etc. that affect topoisomerase II have been shown to produce enzyme linked DNA breaks by trapping a reaction intermediate 'cleavable complex'. This 'cleavage complex' is presumed to be initial event that triggers cellular responses leading to cell death (Topo poisons) [35]. However, cell death can also occur by catalytic inhibitory activity of Topo II targeting drugs by binding to the ATPase domain of Topo II (Topo inhibitors) [36].

2. Results and discussion

2.1. Synthesis and characterzation

Complex **1** was synthesized by reacting methanolic solutions of nalidixic acid (deprotonated with KOH), 1*R*,2*R*–diaminocyclohexane and $ZnCl_2$ as shown in Scheme 1 in a molar ratio of 1:2:1. The synthesized complex was stable towards air and soluble in organic solvents like MeOH, CH_2Cl_2, DMF and DMSO. The molar conductance values of 10^{-3} M solution of complex **1** in DMSO at 25 ºC revealed its 1:1 electrolytic nature. The molecular structure of complex **1** was further established by single crystal X–ray diffraction study. Other analytical techniques used in the characterization of the complex include solution electrical conductivity, FT–IR, UV–vis, NMR (^{1}H and ^{13}C) and ESI–MS techniques that corroborate well with the structure proposed by single crystal X–ray diffraction study.

IR spectroscopy has been used in order to confirm the deprotonation and binding mode of nalidixic acid (HnaI). The IR spectrum of HnaI displayed absorption bands at 3385, 1728 and 1366 cm^{-1} that can be attributed to the ν(O–H), $\nu_{asym}(C=O)_{carboxylic}$ and $\nu_{sym}(C=O)_{carboxylic}$ stretching vibrations, respectively of the carboxylic acid group (–COOH). However, in the IR spectrum of complex **1**, the absence of a peak at 3385 cm^{-1} confirmed the deprotonation of nalidixic acid moiety and its coordination to metal ion. A diagonostic frequency band corresponding to $\nu(NH_2)$ streching vibrations of DACH ligand was found at 3160 cm^{-1}. In addition, the vibration frequency corresponding to $\nu(C=O)_{pyridone}$ was shifted from a value of 1620 (in free HnaI) to 1625 cm^{-1} upon coordination with zinc atom. Further, the characteristic peaks at 1593 and 1388 cm^{-1} were assigned to antisymmetric, $\nu_{asym}(C=O)$ and symmetric, $\nu_{sym}(C=O)$ stretching vibrations of the carboxylato group, respectively. The difference $\Delta\nu = [\nu_{asym}(C=O)-\nu_{sym}(C=O)]$, a useful characteristic aid for predicting the coordination mode of carboxylato ligands suggested a value 205 cm^{-1} for complex **1** which is indicative of monodentate coordination mode for the nalidixic acid moiety [37].

The ^{1}H NMR spectrum of complex **1**, recorded in DMSO–d_6 exhibited characteristic aromatic signatures in the region 8.99–7.39 ppm (H2, H5 and H6). A quartet in the region 4.52 ppm and a triplet at 1.34 ppm were assigned to CH_2 and CH_3 protons of $-NCH_2CH_3$ group, respectively while a sharp singlet corresponding to methyl protons ($ArCH_3$) was observed at 2.63 ppm. Moreover, a complex multiplet in the region 1.63–1.47 and 1.34–1.21 ppm was attributed to DACH ring protons (Fig. S1a).

^{13}C NMR spectrum of the complex **1** revealed carbonyl and carboxylate carbons resonating at 176.71 and 167.22 ppm, respectively. A broad envelope in the range 119–149 ppm was assigned to the aromatic carbons. Additionally, two resonance signals corresponding to CH_2 and CH_3 carbons of $-NCH_2CH_3$ group were found at 49.25 and 14.96 ppm respectively [38].

Cyclohexane ring carbons atoms displayed their resonance signatures in the range 34.89–24.77 ppm (Fig. S1b).

The ESI–MS spectrum (Fig. S2) of complex **1** revealed a molecular ion peak at *m/z* 560.1 attributed to the molecular ion peak, $[C_{24}H_{39}ClN_6O_3Zn]^+$. Fragmentation peaks were observed at *m/z* 527.2 and 297.1 corresponding to $[C_{24}H_{39}N_6O_3Zn–Cl+3H]^+$ and $[C_{24}H_{39}N_6O_3Zn–2DACH+H]^+$ fragments, respectively.

The absorption spectrum of complex **1**, recorded in DMSO at room temperature revealed two well resolved bands, the low energy band centered at 333 nm assigned to n→π* transition and the high energy band at 253 nm attributed to intraligand (IL) π→π* transitions [39].

2.2. Description of the X–ray cyrstal structure

Single crystal X–ray determination at 100 K reveals that complex **1** was successfully solved and converged in the triclinic space group *P*–1. The asymmetric unit of complex **1** contains crystallographically two identical molecules as shown in Fig. S3, while selected bond lengths and bond angles are listed in ESI Table S1. Each molecule in asymmetric unit contain one Zn(II) ion with full occupancy, one ligand unit naI$^-$, two nitrogen–based neutral ligands DACH, two and a half uncoordinated lattice aqua molecules and one chloride ion as illustrated in Fig. 2. Each Zn(II) metal ion shows a distorted octahedral ZnN_4O_2 coordination environment, with ligation from one monodentate carboxylate oxygen and one hydroxyl O atom (Zn–O = 2.027(5)–2.187(7) Å) of ligand unit naI$^-$, four nitrogen atoms from two independent ditopic neutral ligand 1,2–DACH (Zn–N = 2.113(3)–2.124(7) Å). All the Zn–O and Zn–N bond distances are within the range reported for octahedral Zn(II) complexes. A 3D framework has been generated through the multi–point H–bonding interactions between lattice water molecules, non–coordinated carboxylate O atoms interactions between adjacent units as shown in the Fig. S5a and b. The solvent accessible volume again is very high; 37.3% of the total unit cell volume.

2.3. Comparative in vitro Binding Studies of complex **1** *with CT–DNA and tRNA*

Small molecules that show therapeutic potential are most likely to be targeted to DNA rather than RNA and most of the previous studies were pertaining to metal complex–DNA interactions. However unlike DNA, RNA can fold into diverse structures that offer unique binding pockets similar to proteins and can form well–defined structures like double helices, hairpins, bulges, and pseudoknots that could by various therapeutic agents, thus its unique structural diversity could be exploited to design drug entities that specifically target RNA. Metal complexes possessing biologicaly active pharmacophore such as nalidixic acid, can achieve a higher degree of potency by targeting RNA as the bactericidal action of nalidixic acid (quinolones) is also mediated by binding to the bacterial RNA. In lieu of this principle, comparative study of drug candidates towards CT–DNA and tRNA could be instrumental for drug design especially in the area of cancer therapeautics.

2.3.1. UV–vis absorption titrations

In an attempt to investigate the possible binding mode between complex **1** and the nucleic acids (DNA and RNA), the interaction of complex **1** with CT–DNA and yeast tRNA has been studied by UV–vis spectroscopy. With a concomitant increase in the concentration of CT–DNA/yeast tRNA (0.00–5.50 x 10^{-5}M) to a constant concentration of complex **1** (1.11 x 10^{-4} M) resulted in hyperchromism of 31% and 36%, respectively at the intraligand band (Fig. S6a and b). The observed 'hyperchromism' primarily suggested that the complex **1** may bind to CT–DNA/yeast tRNA electrostatically *via* external contact or by possible groove binding. It can be further suggested that the $–NH_2$ and carbonyl oxygen atoms of the complex **1** may involve in hydrogen–bonding interactions with the nucleobases that are accessible both in the major and minor grooves.

In order to elucidate the magnitude of binding strength of complex **1** with these nucleic acids, intrinsic binding constants were calculated by monitoring changes in the absorbance with increasing concentration of DNA/tRNA was determined by using Wolfe–Shimer, Eq. 1

$$\frac{[\text{DNA or RNA}]}{(\varepsilon_a - \varepsilon_f)} = \frac{[\text{DNA or RNA}]}{(\varepsilon_b - \varepsilon_f)} + \frac{1}{K_b(\varepsilon_b - \varepsilon_f)} \quad (\mathbf{1})$$

where [DNA or RNA] are the DNA or RNA concentration, and ε_a, ε_f and ε_b are the apparent (A_{abs}/[complex **1**]), free, and bound complex extinction coefficients respectively. In a plot of [DNA or RNA]/(ε_a–ε_f) vs. [DNA or RNA] with a slope of 1/(ε_b–ε_f) and Y intercept of 1/[K_b(ε_b–ε_f)], K_b value was obtained by the ratio of the slope to the Y intercept. The calculated values of intrinsic binding constants for complex **1** towards CT–DNA or yeast tRNA were found to be 6.16 (±0.09) x 10^4 and 7.49 (±0.13) x 10^4 M^{-1}, respectively.

The K_b values demonstrated stronger binding propensity of **1** towards yeast tRNA owing to fact yeast tRNA which exhibits A–form conformations with L–shaped tertiary structure has a wide shallow minor groove and pulled–in narrow major groove allowing its base pairs to remain well exposed and easily accessible for the drug entities while complex **1** could bind in the bulge region of yeast tRNA, thereby providing a rationale for its stronger binding affinity [40].

2.3.2. Emission spectral studies

In the emission spectra, complex **1** emits luminescence in Tris–HCl buffer pH 7.2 at ambient temperature, with a fluorescence maxima appearing at 347 nm (λ_{ex} = 270 nm). Upon addition of CT–DNA/yeast tRNA (0.00–3.69 x 10^{-5} M) to a fixed concentration of complex **1** (1.67 x 10^{-5} M), enhancement in the fluorescence emission intensity was observed which is indicative of strong interaction with DNA or RNA as depicted in Fig. 3a and b. This enhancement in the emission spectra is largely attributed due to the change in environment from polar to non–polar inside the nucleic acids and is related to the extent to which a

complex gets penetrates into this non–polar hydrophobic environment. Since the hydrophobic environment restricts the complex mobility at its binding site that leads to a decrease in the vibrational modes of relaxation and thus avoids the quenching effects by solvent molecules [41]. The binding constants, *K* as quantified by Scatchard equation were found out to be 6.09 x 10^4 and 7.15 x 10^4 M^{-1} for CT–DNA and yeast tRNA, respectively [42].

To gain more insight about the interaction of complex **1** with CT–DNA and yeast tRNA three–dimensional (3D) fluorescence spectroscopy was also performed on complex **1** both in free form and in the presence of nucleic acids. As shown in Fig. 4, the 3D fluorescence spectrum of **1** consisted of two prominent peaks, peak 1 (λ_{ex}= 380 nm/λ_{em}= 460 nm) and peak 2 (λ_{ex}=270nm/λ_{em}=350nm). However, upon interaction with CT–DNA/tRNA the fluorescence intensity of complex **1** (peak 2) increases significantly; though larger extent in case of yeast tRNA. The results revealed that **1** was efficiently protected inside the hydrophobic environment of RNA than that of DNA and correlated well with other binding studies.

2.3.3. Ethidium bromide displacement assay

To further monitor the interaction mode of complex **1** towards CT–DNA and yeast tRNA, a competitive binding experiment using EB as a probe was carried out. EB emits fluorescence in presence of DNA or RNA due to its strong interaction between the adjacent base pairs. The enhanced fluorescence intensity of EB gets evidently quenched when a second molecule displaces the bound EB molecule from EB–DNA or EB–RNA complex. Thus, the ability of a complex to effect the fluorescence intensity of EB in EB–DNA or EB–RNA adduct can be used as a reliable tool to measure its DNA/RNA binding propensity. EB–DNA/EB–RNA system showed a characteristic strong emission at ca. 587 nm when excited by 450 nm light (Fig. S7a and b). Upon progressive addition of complex **1** to CT–DNA and yeast tRNA, pre–

treated with EB, from a ratio of [complex **1**]/[DNA or RNA] = 1:1 to 8:1, a decrease in emission intensity was observed indicative of competition between EB and complex **1** towards CT–DNA or yeast tRNA binding. However, this decrease in intensity is much lesser as compared to classical intercalators [43], thus ruling out the possibility of intercalative mode. To further quantitatively assess the magnitude of this interaction, classical Stern–Volmer equation was used as

$$I_0/I = 1 + K_{SV}.r \qquad (2)$$

where, I_0 and I represent the fluorescence intensities in the absence and presence of complex **1** respectively; r is the concentration ratio of complex **1** to DNA or RNA and Stern–Volmer constant K_{sv} used to evaluate the quenching efficiency is obtained as the slope of I_0/I *vs* r and was found to be 1.19 and 2.01 for CT–DNA and yeast tRNA, respectively indicating stronger affinity of complex **1** towards RNA than DNA.

2.3.4. Circular dichorism

Circular dichorism (CD) is a sensitive optical technique used to access conformational changes that nucleic acids undergo as a result of complex formation or changes in environment. The CD spectrum of B–DNA exhibits a positive band at 270 nm (UV: λ_{max} 258 nm) due to base stacking and a negative band at 245 nm due to the right–handed helicity, which are quite sensitive to the mode of DNA interactions with small molecules. Simple groove binding and electrostatic interaction of the complex with CT–DNA shows less or no perturbation of the base stacking and helicity bands, while an intercalator enhances the intensities of both bands [44]. Upon addition of complex **1** to CT–DNA, ([complex **1**]/[DNA] = 1), the CD spectrum undergoes decrease in intensity in both the positive (helicity) and negative (ellipticity) bands (Fig. S8a). The decrease in the intensity in positive and negative

bands suggests that the complex **1** can unwind the DNA helix that leads to loss of helicity [45].

On the contrary, the CD spectrum of tRNA depicts characteristic four major peaks at 210 and 243 nm (negative), 225 and 270 nm (positive) consistent with the CD spectrum of A–conformation of tRNA. Upon addition of complex **1** to tRNA solution ([complex **1**]/[DNA] = 1) a significant increase in the intensity of a negative band at 212 nm was observed while positive bands at 225 and 270 nm showed relatively less decrease in intensities with less or no band shifting (Fig. S8b). The major alterations in the intensity of 212 nm band could be due to reduction in base stacking interactions and tRNA aggregation upon addition of complex **1** that is a typical of A–form RNA conformation [46].

2.3.5. Viscometric measurements

Viscosity experiment is an effective tool to clarify the binding modes between small molecules and DNA. Well–known DNA intercalators like EB, causes DNA helix to increase its length by separating its base pairs to accommodate itself, resulting an increase in viscosity. However, complexes that bind either electrostatically *via* sugar–phosphate backbone may produce bends or kinks in the DNA helix reducing its effective length and viscosity, while DNA groove binding under the identical experimental conditions essentially results in less or no effect on DNA viscosity [47].

Plots of relative viscosity $(\eta/\eta_o)^{1/3}$ vs. [Compound]/[DNA] shown in Fig. S9 exhibited a decrease in relative specific viscosity suggesting the non–intercalative interaction, *viz.*, electrostatic binding of complex **1** towards CT–DNA. While in case of EB, the viscosity increased notably upon increasing its concentration suggestive of intercalation as a binding mode [48]. In contrast, no obvious change in relative viscosity was observed for yeast tRNA upon addition of complex **1** owing to its non–linear L–shaped tertiary structure [49].

2.4. pBR322 DNA cleavage studies

In order to assess the cleavage activity of pBR322 DNA by complex **1**, agarose gel electrophoretic mobility assay was performed using pBR322 plasmid DNA as a substrate in a medium of 5 mM Tris–HCl/50 mM NaCl buffer, at pH 7.2. It is well known that DNA cleavage is reflected by relaxation of the supercoiled circular form (Form I) of pBR322 DNA resulting in nicked circular (Form II) and/or linear forms (Form III). Zinc ion is regarded as one of the best suited metal ion for the development of artificial metallonucleases; catalyzing hydrolytic cleavage of DNA due to its strong Lewis acid and redox inert nature, it was therefore imperative to study the effect of Zn(II) complex on pBR322 DNA cleavage [50]. The DNA cleavage ability of complex **1** was performed where pBR322 DNA was incubated with increasing concentration (15–35 μM) of **1** in buffer for 45 min (Fig. 5). With increasing concentrations of the complex **1** (Lanes 2–6), the amount of Form I of pBR322 DNA diminishes gradually, whereas Form II increases without the formation of Form III, suggesting single strand DNA cleavage.

Mechanistic investigations were done using reactive oxygen species (ROS) such as hydroxyl radical scavengers (DMSO and EtOH), singlet oxygen scavenger (NaN_3) and a superoxide scavenger (SOD) involved in the DNA cleavage reactions (Fig. 6). The experiment results showed that the DNA breakdown mediated by complex **1** was clearly inhibited in the presence of DMSO and EtOH (Lanes 2 and 3), indicating that OH free radicals participate in the oxidation of the deoxyribose moiety, followed by hydrolytic cleavage of the sugar phosphate backbone of DNA. On the other hand, addition of NaN_3 and SOD (Lanes 4 and 5) did not show any significant inhibition of the DNA strand scission, and even in presence of NaN_3 and SOD, the cleavage reaction was enhanced suggesting the non–involvement of the singlet oxygen radical and superoxide anion radical in the mechanistic pathway of DNA cleavage. Since, hydrolysis promoted by metal ions mainly depends on the Lewis acidity, which serves to activate the phosphodiester bonds towards nucleophilic attack

via charge neutralization. This hypothesis is consistent with previous literature reports which reveals that Zn(II) complexes generally cleave the DNA by hydrolytic pathway.

The potential interacting site of complex **1** with pBR322 DNA was determined in presence of minor groove binding agent (DAPI and distamycin) and the major groove binding agent (methyl green). When supercoiled pBR322 was treated with these agents prior to the addition of complex **1**, the cleavage reaction mediated by **1** was quenched in presence of minor groove binding agent (Lanes 6 and 7) while it was enhanced in the presence of methyl green (Lane 8) indicating minor groove–binding preference of complex **1**.

2.5. T4 DNA religation assay

To ascertain the hydrolytic nature of the DNA cleavage reaction mediated by complex **1**, DNA religation experiment was performed in which supercoiled pBR322 DNA was treated with T4 DNA ligase enzyme and subjected to gel electrophoresis. It is well known that in DNA hydrolytic cleavage 3′–OH and 5′–OPO_3 (5′–OH and 3′–phosphate) fragments are formed exclusively and that these fragments can be enzymatically ligated. In some cases, the hydrolytic products either did not end at the required 5′–phosphate and 3′–OH (ribose) termini or the complex is sometimes bound to the termini of cleaved DNA. These reasons would result in the religation being incomplete or even failing completely [51,52]. The complex **1** yielded nicked DNA which was religated by using T4 DNA ligase enzyme; nicked form (Form II) was religated to a large extent in the presence of T4 ligase enzyme in comparison to control DNA alone in supercoiled form (Fig. S10). Complex **1** could therefore, be useful not only in drug design but also in elucidating the precise role of metal ions in enzyme catalysis.

2.6. RNA cleavage

Synthetic nucleases that specifically cleave and target RNA promote the selective inhibition of protein expression in cell culture which can have potential therapeutic benefits [53,54].

Generally, metal complexes have been used as an effective mediators of hydrolytic cleavage of the RNA phosphate ester backbone and thus can be utilized in modeling and elucidation of the mechanism of metal ion catalyzed cleavage of RNA by biological catalysts. To investigate the mechanism of RNA cleavage, we analyzed the results of cleavage assays using agarose gel electrophoresis in a time dependent manner. Briefly, tRNA was mixed with different concentrations of complex **1** and the mixture was incubated at 37 °C with respect to different time interval (Fig. 7a and b). The gel electrophoretic results revealed that after 2h of incubation, the complex **1** induced RNA cleavage was inhibited and intensity of the bands was affected in presence of increasing complex concentrations (6.25–19.37 μM). At the same time, when the concentration of complex **1** reached 12.5 μM, the gel mobility of RNA was slightly retarded which resulted in partial blockage of the RNA mobility through the porous gel due to the electrostatic interactions between the complex **1** and the negatively charged RNA phosphate backbone resulting in neutralization of the negative charges [55]. However, complete degradation of RNA cleavage was observed after 24h of incubation, followed by the complete absence of the RNA band.

2.7. Topoisomerase II inhibitory activity

Topoisomerase II is one of the nuclear enzyme that controls the topology (or conformation) of a DNA segment and acts by introducing transient break in both strands of DNA to generate a staggered double–strand DNA and requires ATP [56]. The expression of this enzyme is generally elevated in rapidly proliferating tumor cells, therefore, Topo–II targeting agents have long been considered as an attractive intracellular target for the design of cancer chemotherapeutics because they can cause permanent DNA damage that triggers a series of cellular events, inducing apoptosis and finally causing cell death [57].

The effect of concentration–dependent Topo–II inhibition assay of complex **1** was performed in the enzyme–mediated supercoiled pBR322 DNA relaxation assay in the presence of ATP

using agarose gel electrophoresis. When enzymatic activity was assayed, supercoiled plasmid DNA was converted to relaxed circular form and then yielded linear DNA. The presence of each type of DNA indicates a different behavior by the enzyme: relaxed DNA reveals that the enzyme's isomerase activity remains intact; supercoiled DNA suggests that the enzyme's action was inhibited; linear DNA reveals the formation of permanent double strand breaks during the catalytic cycle [36]. As shown in Fig. 8, it was observed that the treatment with 5μM (Lane 3) of complex **1** afforded partial inhibitory activity. As the concentration increases (10–30 μM), complex **1** successively inhibited the DNA relaxation activity of Topo II. These experiments implicate that **1** exhibited Topo–II inhibition, revealing a promising effect *via* binding to the ATPase domain of Topo II due to the presence of hydrogen bonding donor and acceptor moieties which may anchor in the entrance of ATP–binding pocket resulting in increased binding affinity, thereby leads to a higher Topo–II catalytic inhibitory activity. Thus, we conclude that complex **1** was catalytic inhibitor and not topoisomerase poisons because topoisomerase poisons give rise to permanent DNA cleavage by binding to the Topo–DNA complex covalently. On other hand, Topo–II catalytic inhibitors interact non–covalently with enzyme (e.g. substrate competition) to impede enzymatic activity during the catalytic cycle, thus, alter their normal functioning resulting in cell death.

2.8. Molecular docking

2.8.1. Molecular docking with DNA and RNA targets

In order to get more insight into the mode of binding and affinity, complex **1** was docked with DNA duplex of sequence d(CGCGAATTCGCG)$_2$ dodecamer (PDB ID:1BNA). The minimum energy docked pose shows that complex **1** interacts with DNA *via* outside edge interactions mainly through DACH rings inside the GC region of DNA minor groove, stabilized by hydrogen bonding between NH_2 group of complex **1** and O(P2) of G14 from chain A of DNA double helix. Another amino group from DACH ring was also involved in

hydrogen bonding interaction with C–3 carbonyl oxygen of Cyt11, while the nalidixic acid moiety slightly bends the DNA in such a way that a part of the nalidixic acid ring moiety makes favourable stacking interactions between DNA base pairs leading to van der Waals interaction and hydrophobic contacts (Fig. 9).

Complex **1** was also successively docked towards the molecular target HIV–1 TAR RNA (PDB ID: 1UUI) in order to substantiate the experimental observation. It is well known that TAR RNA has a well defined 3D structures including unpaired bulges (21–25), unpaired loops (10–15), paired upper (16–40) and lower stem (41–49) (Fig. 10a). These structural motifs participate directly or indirectly with the targets for specific recognition process [58]. The resulting docked model implied that complex **1** was inserted into the active pocket located between upper and lower stem and was in close proximity of G–17, G–18, C–19, A–22, U–40, C–41, U–42. The structural features of **1** allows it to form multiple intermolecular H–bonds between carbonyl 'O' atom of nalidixic acid moiety and N4 of U–42 (2.4 A°) whereas, NH_2 group of DACH ring interacts with the O6 of A–22 (3.1 A°) and the phosphate back bone of the RNA strand (Fig. 10b). In addition these interactions are further stabilized by the van der Waal interactions.

The resulting relative binding energy of docked complex **1** with DNA and RNA was found to be –270.3 and –289.7 KJ mol^{-1}, respectively, indicating the complex **1** has more affinity for tRNA in comparison to CT–DNA, consistent with the spectroscopic results.

2.8.2. Molecular docking with Topo–II

To study the molecular basis of interaction and rationalize the observed enzymatic activity, molecular docking studies of complex **1** with the ATP–binding domain of human Topo–IIα (PDB ID: 1ZXM) was carried out. The docking model showed that complex **1** was approaching towards the middle of ATP binding pocket and stabilized by strong hydrophobic interactions with Asn91, Asn95, Lys121, Gln60, Gln310 and Met61 residues (Fig. 11). Other

hydrophobic residues such as Ile311, Ile118 and Gln310 form a small subpocket at the bottom of the binding site filled with water molecules that establish a hydrogen bond network connecting the side chain of Asn120 to that of Asn91 [59]. On the opposite side three residues, Ile125 together with Arg98 and Ser149, constitute the entrance of the cavity. Moreover, the carbonyl oxygen atom and the NH_2 group of complex **1** forms hydrogen bonds with Trp72, Gln59 and Met61 in addition to their π–π interaction between aromatic ring of the complex **1** and ATP–binding site and magnesium ion. These multiple interactions between complex **1** and residues in the ATPase domain and the magnesium ion suggest that the metal complex can form a strong binding interaction with Topo II, preventing the entry of ATP [60]. The resulting binding energy of docked complex with DNA binding site of topoisomerase II and ATP domain were found to be −278.9 and −304.7 KJ mol^{-1}, respectively indicating better affinity towards the ATP pocket than for the DNA binding site than for the DNA binding site.

3. Conclusion

In this work, we have synthesized a new Zn(II) complex **1** derived from the Nalidixic acid and 1*R*,2*R*–diaminocyclohexane as metallo drug to act as a potential antitumor agent. Complex **1** was characterized by elemental analysis, IR, UV–vis, molar conductance measurements and single X–ray crystallography. The *in vitro* DNA/RNA binding studies of complex **1** revealed an electrostatic mode of binding as well as selectively bind to minor groove of DNA and bulge region of RNA. The gel electrophoresis results showed that complex **1** induced the pBR322 DNA cleavage pattern through a hydrolytic cleavage mechanism which was supported by evidence from DNA relegation employing T4 DNA ligase assay. Among the exceptional biological properties, notably important Topo–II inhibition assay suggested that **1** was catalytic inhibitor of human Topo–II at a concentration of 30 μM. Additionally, molecular docking studies were performed with molecular target

DNA, RNA and the active site of Topo–II in order to validate the experimental results. These studies suggest that a metal could synergistically tune the biological properties of ligand scaffold and is therefore, instrumental for the design of a potential chemotherapeutic drug.

4. Experimental section

4.1. Reagents and materials

Commercially obtained chemicals were used as received without further purification. Nalidixic acid (Sigma Aldrich), 1*R*,2*R*–diaminocyclohexane from Sigma Aldrich (DACH), Zinc chloride, tris–(hydroxymethyl)aminomethane (tris–buffer) (Merck). Calf thymus DNA (CT–DNA) and yeast RNA (Type IX from Torula yeast) were purchased from Sigma Co. and were stored at 4 °C, 6X loading dye (Fermental Life Science) and Supercoiled plasmid DNA pBR322 (Genei), T4 DNA ligase enzyme and Human–Topoisomerase–II enzyme (CalBioChem).

4.2. Methods and instrumentation

Elemental analysis was carried out on Carlo Erba Analyser Model 1106. Molar conductance was measured at room temperature on Eutech con 510 electronic conductivity bridge. Fourier–transform infrared (FT–IR) spectra were recorded on an Interspec 2020 FT–IR spectrometer. ESI–MS spectra were recorded on Micromass Quattro II triple quadrupole mass spectrometer. NMR spectra were obtained on a Bruker DRX–400 spectrometer with Me_2SO–d_6 as solvent. Electronic spectra were recorded on UV–1700 PharmaSpec UV–vis spectrophotometer (Shimadzu) in DMSO using cuvettes of 1 cm path length and data were reported in λ_{max}/nm. Emission spectra were made on Shimadzu RF–5301PC/Hitachi F-2700 Spectrofluorophotometers. All the experiments involving the interaction of the complex with CT–DNA and the yeast tRNA were carried out in aerated buffer (5mM Tris–HCl, 50mM NaCl, pH = 7.2). The concentration per base pairs for both DNA and RNA was determined spectrophotometrically by assuming ε_{260nm} values to be 6600 and 7700 $M^{-1}cm^{-1}$ respectively.

CD spectra were measured on Jasco J–815–CD spectropolarimeter at room temperature. The viscosity measurements were carried out using Oswald capillary viscometer maintained at 25 °C. Cleavage experiments were performed with the help of Axygen electrophoresis supported by a Genei power supply with a potential range of 50–500 V, visualized and photographed by Vilber–INFINITY gel documentation system.

4.3. Synthesis of [Zn(naI)(DACH)$_2$]Cl (**1**)

Nalidixic acid (HnaI) (0.464 g, 2 mmol) was suspended in MeOH, and KOH (0.112 g, 2 mmol) was added to it followed by a methanolic solution of $ZnCl_2$ (0.272 g, 2 mmol). After 0.5h of stirring a methanolic solution of 1*R*,2*R*–diaminocyclohexane (0.456 g, 4 mmol) was added drop wise and the reaction mixture was further kept on stirring for ca. 3h to yield a white colored precipitate which was filtered, washed with hexane and dried under vacuum. Suitable crystals for single X–ray crystallography analysis were obtained after recrystallization from the mixture of MeOH–$CHCl_3$ in 8:2 ratio (CCDC: 901439).

Yield: 76%. m.p. 177 ºC (dec.): Molar Conductance (DMSO): Λ_M = 71.03 $\Omega^{-1}cm^2mol^{-1}$ (1:1 electrolyte). Anal. Calcd. for $[C_{24}H_{39}N_6O_3Zn]Cl$ (%): C, 51.43; H, 7.01; N, 15.01: Found C, 51.57; H, 7.11; N, 14.91. IR (KBr, ν_{max}/cm^{-1}): 3160 $\nu(-NH_2)$; 1625 $\nu(C=O)_{pyridone}$; 1593 $\nu_{asym}(C=O)$; 1388 ν_{sym} (C=O), 728 ν(Ar): ^{1}H NMR (400 MHz, DMSO–d_6, δ, ppm): 8.99 (s, 1H, H2), 8.44 (d,1H, H5), 7.41 (d, 1H, H6), 4.52 (q, 2H, NCH_2CH$_3$), 3.35 (s, 4H, –NH_2), 2.63 (s, 3H, ArCH_3), 1.63–1.47 and 1.34–1.21 (complex m, 8H, –CH_2– of cyclohexyl), 1.39 (t, 3H, –NCH$_2$CH_3). ^{13}C NMR (100 MHz, DMSO–d_6, δ, ppm): 176.71 (C–4), 167.55 (C–11), 162.73 (C–7), 149.50 (C–2), 147.60 (C–9), 135.86 (C–5), 120.79 (C–6), 119.42 (C–10), 49.25 (C–12), 34.89 (–CH– cyclohexyl), 28.05–24.77 (–CH$_2$ cyclohexyl ring carbons), C–13 14.96. ESI–MS (*m/z*): 560 $[C_{24}H_{39}ClN_6O_3Zn]^+$.

4.4. Description of X–ray Crystal structure

Suitable X–ray quality crystals of the complex **1** were obtained after slow evaporation of the reaction mixture at room temperature. Single crystal X–ray structural studies of complex was performed on a CCD Oxford Diffraction Xcalibur Saphir 3 diffractometer employing graphite–monochromated Mo–Kα radiation generated from a fine–focus sealed tube (λ=0.71073Å) at 140(2) K. Data collection strategy was evaluated by using the CrysAlisPro CCD software. Collections of data were observed by the standard ω scan techniques and were scaled and reduced using CrysAlisPro RED software. The structure was solved by direct methods using SIR–97 [61] and refined by least–squares methods on F^2 using SHELXL–97 [62]. The positions of all atoms were obtained by direct methods. Anisotropic thermal parameter were assigned to all non–hydrogen atoms and the remaining hydrogen atoms were placed in geometrically constrained position and refined as riding atoms with a common fixed isotropic thermal parameter. The drawing of the complex was realized with PLATON [63]. A summary of the selected crystallographic information is given in Table 2.

4.5. DNA/RNA binding and cleavage experiments

DNA binding experiments include absorption spectral traces, emission spectroscopy, viscosity measurements and CD conformed to the standard methods and practices previously adopted by our laboratory [64–67]. RNA binding studies was performed in Tris–HCl/NaCl (5:50 mM) buffer at pH 7.2 which includes absorption titration, emission spectroscopy and CD measurement according to the protocol described previously. While measuring the absorption spectra an equal amount of DNA/RNA was added to both the compound solution and the reference solution to eliminate the absorbance of the CT–DNA/tRNA itself, and Tris buffer was subtracted through base line correction.

The cleavage experiments of supercoiled pBR322 DNA (300 ng) by complex **1** in Tris–HCl/NaCl (5:50 mM) buffer at pH 7.2 was carried out using agarose gel electrophoresis. The samples were incubated for 45 min at 37 ºC. The DNA cleavage with added reductant was

monitored as in case of cleavage experiment without added reductant using agarose gel electrophoresis. A loading buffer containing 25% bromophenol blue, 0.25% xylene cyanol, 30% glycerol was added and electrophoresis was carried out at 50 V for 1h in Tris–HCl buffer using 1% agarose gel containing 1.0 mg/ml ethidium bromide.

The RNA cleavage reaction was performed in a Tris–HCl 40 mM, pH 8.0 buffer. The reaction mixture containing increasing concentration of complex **1** was incubated for 2 h and 24h at 37 $^{\circ}$C. The electrophoresis was performed using TBE (Tris Borate–EDTA) buffer buffer for 200 min at 5 V/cm. The gel was then soaked 20 min with and rinsed 30 min in distilled water. RNA fragments were visualized, after an incubation with EB (0.5 mg/mL), using an UV transilluminator [68].

4.6. Religation experiment with T4 DNA ligase enzyme

The DNA religation experiments were performed using T4 DNA ligase enzyme to support the hydrolytic mechanism of DNA cleavage by following the standard DNA religation protocol. Complex **1** treated with pBR322 plasmid DNA, ligation buffer of 1.5mL in 10X, T4 DNA ligase, 1 mL (2 units) and 2.5 mL of H_2O were mixed and incubated at 4 ºC for 1h. Subsequently, the samples were loaded on 1% agarose gel and visualized by staining with EB solution.

4.7. Topoisomerase Inhibition Assay

DNA topoisomerase IIα (Topo II) was purchased from Sigma and no further purification was performed. One unit of the enzyme was defined as completely relax 0.3µg of negatively supercoiled pBR322 DNA in 15 min at 37 °C under the standard assay conditions. The reaction mixture (30 µL) contained 10 mM Tris–HCl (pH 7.9), 50 mM NaCl, 50 mM KCl, 5.0 mM $MgCl_2$, 0.1 mM Na_2H_2edta, 15µg/mL BSA, 1.0 mM ATP, 0.25µg pBR322 DNA, 5 Unit Topo II, and complex **1**. The samples were electrophoresed through 1% agarose in TBE at 30V for 8h.

4.8. Molecular docking studies

The rigid molecular docking studies were performed by using HEX 6.1 software [69], which is an interactive molecular graphics program for calculating and displaying feasible docking modes of an enzymes and DNA molecule. The crystal structure of the B–DNA dodecamer d(CGCGAATTCGCG)$_2$ (PDB ID: 1BNA), RNA (PDB ID: 1UUI) and human–DNA–Topo–II (PDB ID: 1ZXM) were downloaded from the protein data bank (http://www.rcsb.org./pdb). Visualization of the docked pose has been done by using CHIMERA (www.cgl.ucsf.edu/chimera) and PYMOL (http://pymol.sourceforge.net/) and Discovery Studio molecular graphics program.

Acknowledgements

The authors are grateful to *SAIF*, Panjab University, Chandigarh and *STIC*, Cochin University, Cochin for providing ESI–MS, NMR and elemental analysis facility, respectively. The author (I. Yousuf) expresses his gratitude to *University Grants Commission* (UGC), New Delhi, for Junior Research Fellowship.

Appendix A: Supplementary Information

Crystallographic data is also available from the CCDC as file CCDC 901439.

References

[1] D. Li, S. Song, C. Fan, Acc. Chem. Res. 43 (2010) 631.

[2] D.M. Kolpashchikov, Chem. Rev. 110 (2010) 4709.

[3] M. Gaglione, G. Milano, A. Chambery, L. Moggio, A. Romanelli A. Messere, Mol. Biosyst. 7 (2011) 2490.

[4] J.–H. Li, J.–T. Wang, Z.–W. Mao L.–N. Ji, Inorg. Chem. Comm. 11 (2008) 865.

[5] D. Desbouis, I.P. Troitsky, M.J. Belousoff, L. Spiccia, B. Graham, Coord. Chem. Rev. 256 (2012) 897.

[6] T.W. Hambley, Dalton Trans. (2007) 4929.

[7] C.X. Zhang, S.J. Lippard, Curr. Opin. Chem. Biol. 7 (2003) 481.

[8] S.P. Fricker, Dalton Trans. (2007) 4903.

[9] J. Gallego, G. Varani, Acc. Chem. Res. 34 (2001) 836.

[10] N. Foloppe, N. Matassova, F. Aboul–ela, Drug Discov. Today 11 (2006) 1019.

[11] R.W.–Y. Sun, D.–L. Ma, E. L.–M. Wong, C.–M. Che, Dalton Trans. (2007) 4884.

[12] J.–H. Wen, C.–Y. Li, Z.–R. Geng, X.–Y. Ma, Z.–L. Wang, Chem. Commun. 47 (2011) 11330.

[13] C.G. Hartinger, N.M.–Nolte, P.J. Dyson, Organometallics 31 (2012) 5677.

[14] S.P. Fricker, Dalton Trans. (2007) 4903.

[15] M.A. Fuertes, C. Alonso, J. M. Perez, Chem. Rev. 103 (2003) 645.

[16] S.S. Hah, R.A. Sumbad, R.W.V. White, K.W. Turteltaub, P.T. Henderson, Chem. Res. Toxicol. 20 (2007) 17451.

[17] C. Manzotti, G. Pratesi, E. Menta, R.D. Domenico, E. Cavalletti, H.H. Fiebig, L.R. Kelland, N. Farrell, D. Polizzi, R. Supino, G. Pezzoni, F. Zunino, Clin. Cancer Res. 6 (2000) 2626.

[18] G. Sava, S. Zorzet, C. Turrin, F. Vita, M. Soranzo, G. Zabucchi, M. Cocchietto, A. Bergamo, S. DiGiovine, G. Pezzoni, L. Sartor, S. Garbisa, Clin. Cancer Res. 9 (2003) 1898.

[19] V.B. Arion, R. Erwin, M. Fremuth, M.A. Jakupec, B.K. Keppler, Y.K. Vadim, A.J.L. Pombeiro, Inorg. Chem. 42 (2003) 6024.

[20] J.D. Hoeschele, A. Habtemariam, J. Muir, P. Sadler, Dalton Trans. (2007) 4974.

[21] P. F. Liguori, A. Valentini, M. Palma, A. Bellusci, S. Bernardini, M. Ghedini, M.L. Panno, C. Pettinari, F. Marchetti, A. Crispini, D. Pucci, Dalton Trans. 39 (2010) 4205.

[22] L. Guan, M.D. Disney, ACS Chem. Biol. 7 (2012) 73.

[23] C.F. Bennett, E.E. Swayze, Annu. Rev. Pharmacol. Toxicol. 50 (2010) 259.

[24] H.K. Liu, P.J. Sadler, Acc. Chem. Res. 44 (2011) 349.

[25] M. Chauhan, K. Banerjee, F. Arjmand, Inorg. Chem. 46 (2007) 3072.

[26] S. Neidle, Nat. Prod. Rep. 18 (2001) 291.

[27] C.S. Chow, F.M. Bogdan, Chem. Rev. 97 (1997) 1489.

[28] T. Storr, K.H. Thompson, C. Orvig, Chem. Soc. Rev. 35 (2006) 534.

[29] F.R. Keene, J.A. Smith, J.G. Collins, Coord. Chem. Rev. 253 (2009) 2021.

[30] C. Sanchez, P. Belleville, M. Popall, L. Nicole, Chem. Soc. Rev. 40 (2011) 696.

[31] K.B. Turner, A.S. Kohlway, N.A. Hagan, D. Fabris, Biopolymers 91 (2008) 283.

[32] L.L. Shen, J. Baranowski, A.G. Pernet, Biochemistry 28 (1989) 3879.

[33] S. Liu, W. Cao, L. Yu, W. Zheng, L. Li, C. Fana, T. Chen, Dalton Trans. 42 (2013) 5932.

[34] G. Psomas, D.P. Kessissoglou, Dalton Trans. 42 (2013) 6252.

[35] F. Liu, Annu. Rev. Biochem. 58 (1989) 351.

[36] K. Suzuki, F. Shono, M. Uyeda, Biosci. Biotechnol. Biochem. 66 (2002) 1706.

[37] C.D.–Samara, G. Tsotsou, L.V. Ekateriniadou, A.H. Kortsaris, C.P. Raptopoulou, A. Terzis, D.A. Kyriakidis, D.P. Kessissoglou, J. Inorg. Biochem. 71 (1998) 171.

[38] J. Kljun, I. Bratsos, E. Alessio, G. Psomas, U. Repnik, M. Butinar, B. Turk, I. Turel, Inorg. Chem. 52 (2013) 9039.

[39] A. Tarushi, G. Psomas, C.P. Raptopoulou, D.P. Kessissoglou, J. Inorg. Biochem. 101 (2009) 898.

[40] X. Liang, X. Zou, L. Tan, W. Zhu, J. Inorg. Biochem. 104 (2010) 1259.

[41] S. Tabassum, M. Zaki, M. Afzal, F. Arjmand, Dalton Trans. 42 (2013) 10029.

[42] F. Cui, Y. Yan, Q. Zhang, J. Du, X. Yao, G. Qu, Y. Lu, Carbohydr. Res. 344 (2009) 642.

[43] N.W. Luedtke, J.S. Hwang, E. Nava, D. Gut, M. Kol, Y. Tor, Nucl. Acids Res. 31 (2003) 5732.

[44] F. Arjmand, S. Parveen, D. K. Mohapatra, Inorg. Chim. Acta 388 (2012) 1.

[45] K. Karidi, A. Garoufis, N. Hadjiliadis, J. Reedijk, Dalton Trans. (2005) 728.

[46] C.N.N. soukpoe–Kossi, C. Descoteaux, E. Asselin, J. Bariyanga, H.–A. Tajmir–Riahi, G. Berube, DNA Cell Biol. 27 (2008) 337.

[47] F. Arjmand, M. Muddassir, Chirality 23 (2011) 250.

[48] S. Mahadevan, M. Palaniandavar, Inorg. Chem. 37 (1998) 693.

[49] H. Xu, Y. Liang, P. Zhang, F. Du, B.–R. Zhou, J. Wu, J.–H. Liu, Z.–G. Liu, L.–N. Ji, J. Biol. Inorg. Chem. 10 (2005) 529.

[50] F. Mancin P. Scrimin, P. Tecilla, U. Tonellato, Chem. Commun. 2005, 2540.

[51] M. Scarpellini, A. Neves, R. Horner, A.J. Bortoluzzi, B. Szpoganics, C. Zucco, R.A. N. Silva, V. Drago, A.S. Mangrich, W.A. Ortiz, W.A.C. Passos, M.C.B. de Oliveira, H. Terenzi, Inorg. Chem. 42 (2003) 8353.

[52] C. Sissi, F. Mancin, M. Gatos, M. Palumbo, P. Tecilla, U. Tonellato, Inorg. Chem. 44 (2005) 2310.

[53] B.F. Baker, S.S. Lot, J. Kringel, S. Cheng–Flournoy, P. Villiet, H.M. Sasmor, A.M. Siwkowski, L.L. Chappell, J.R. Morrow, Nucl. Acids Res. 27 (1999) 1547.

[54] C.–A. Chen, J.A. Cowan, Chem. Commun. (2002) 196.

[55] S.M. Freier, K.–H. Altmann, Nucl. Acids Res. 25 (1997) 4429.

[56] U. Kellner, P. Rudolph, R. Parwaresch, Onkologie 23 (2000) 424.

[57] W. Shi, S.L. Marcus, T.L. Lowary, Bioorg. Med. Chem. 19 (2011) 603.

[58] R. Pang, C. Zhang, D. Yuan, M. Yang, Bioorg. Med. Chem. 16 (2008) 8178.

[59] P. Furet, J. Schoepfer, T. Radimerski, P. Chène, Bioorg. Med. Chem. Lett. 19 (2009) 4014.

[60] C.–X. Hu, Z.–L. Zuo, B. Xiong, J.–G. Ma, M.–Y. Geng, L.–P. Lin, H.–L. Jiang, J. Ding, Mol. Pharmacol.70 (2006) 1593.

[61] G.M. Sheldrick, SHELX–97, Program for Crystal Structure refinement, University of Göttingen, Germany, 1997.

[62] G.M. Sheldrick, SHELX–97, Program for Crystal Structure refinement, University of Göttingen, Germany, 1997.

[63] A.L. Spek, PLATON Procedure, A multipurpose Crystallographic Tool, Utrecht University, Utrecht, The Netherlands, 1998.

[64] M.E. Reicmann, S.A. Rice, C.A. Thomas, P. Doty, J. Am. Chem. Soc. 76 (1954) 3047.

[65] A. Wolfe, G.H. Shimer, T. Meehan, Biochemistry 26 (1987) 6392.

[66] J.R. Lakowiez, G. Webber, Biochemistry 12 (1973) 4161.

[67] F. Arjmand, M. Muddassir, Y. Zaidi, D. Ray, Med. Chem. Commun. 14 (2011) 394.

[68] M. Marketaki, E. Touloupakis, G. Charalambidis, M.–C. Chalbot, D.F. Ghanotakis, A.G. Coutsolelos, J. Porphyrins Phthalocyanines 16 (2012) 1.

[69] D. Mustard, D.W. Ritchie, Proteins: Struct. Funct. Bioinf. 60 (2005) 269.

Figure Captions

Fig.1. Schematic representations of (a) nalidixic acid along with its numbering scheme (b) Proposed model of complex **1** along with its specific domains.

Fig.2. Diagram showing a single asymmetric unit of complex **1**

Fig.3. Emission spectra of complex **1** in Tris–HCl buffer at pH 7.2 upon addition (a) CT–DNA, (b) yeast tRNA; [DNA], [RNA] = 0.00–3.69 x 10^{-5} M. [Complex 1] = 1.67 x 10^{-5} M. Arrow shows change in intensity with increasing concentration of DNA/RNA.

Fig.4. 3D fluorescence spectra of (a) free complex **1**; (b) complex **1** in presence of CT–DNA and (c) complex **1** in presence of yeast tRNA**.** The concentration of complex was 3.2 x 10^{-4} M and that of CT–DNA and yeast tRNA was 2.2 x 10^{-4} M.

Fig.5. Agarose gel electrophoresis showing cleavage of pBR322 supercoiled DNA (300 ng) by complex **1** at 37 ºC after 45 min of incubation at different concentrations; Lane 1: DNA control; Lane 2: 15 μM of **1**+DNA**;** Lane 3: 20 μM of **1**+DNA; Lane 4: 25 μM of **1**+DNA; Lane 5: 30 μM of **1**+DNA; Lane 6: 35 μM of **1**+DNA.

Fig.6. Agarose gel electrophoresis showing cleavage of pBR322 supercoiled DNA (300 ng) by complex **1** (30 μM) at 37 ºC after 45 min of incubation in presence different radical scavengers and groove binders. Lane 1: DNA control; Lane 2: **1**+DMSO (0.4 M)+DNA; Lane 3: **1**+Ethyl alcohol (0.4 M)+DNA; Lane 4: **1**+sodium azide (0.4 M) + DNA; Lane 5: **1**+SOD (15 units)+DNA; Lane 6: **1**+DAPI (8 μM) + DNA: Lane 7: **1**+distamycin (100 μM)+DNA; Lane 8: **1**+methyl green (2.5 μL of a 0.01mg/ml solution)+DNA.

Fig.7. Agarose gel electrophoresis showing RNA cleavage after (a) 2h and (b) 24h of incubation time at 37 ºC with increasing concentrations of complex **1** in a Tris–HCl 40 mM, pH 8.0 in TBE buffer. Lane 1: RNA control; Lane 2: 6.25 μM of **1**+RNA; Lane 3: 9.25 μM of **1**+RNA; Lane 4: 12.37 μM of **1**+RNA; Lane 5: 15.87 μM of **1**+RNA; Lane 6: 19.37 μM of **1**+RNA.

Fig.8. Agarose gel electrophoresis showing effect of different concentrations of complex **1** on the activity of human–DNA Topo IIα (Topo–II, 5 units); Lane 1: DNA control; Lane 2: Topo–II control (Topo–II + DNA); Lane 3: 5 μM of **1**+DNA+Topo–II; Lane 4: 10 μM of **1**+DNA+Topo–II; Lane 5: 15 μM of **1**+DNA+Topo–II; Lane 6: 20 μM of **1**+DNA+Topo–II; Lane 7: 25 μM of **1**+DNA; Lane 8: 30 μM of **1**+DNA

Fig.9. Molecular docked model of complex **1** fitted into GC base pairs from minor groove side with DNA dodecamer duplex of sequence d$(CGCGAATTCGCG)_2$ (PDB ID: 1BNA).

Fig.10. (a) Schematic representation of a loop, bulge and stem secondary structure of HIV–1 TAR RNA (PDB ID: 1UUI). The unpaired bulge is numbered 23–25. (b) Docking structure between TAR RNA (PDB ID: 1UUI) and complex **1**.

Fig.11. Molecular docked model of complex **1** in to the ATP binding pocket of human Topo IIα (a) The ATP–binding domain was shown in a cartoon (b) The ATP–binding domain is represented as a molecular surface, and complex **1** in ball and stick

representation, (PDB ID:1ZXM). (c) The hydrogen bonding network at the top of the active site in the docked model of complex **1** and Topo IIα. Hydrogen bonds are represented by dashed lines and the distances between them are indicated.

Table 1: Limitations of some prominent anticancer agents.

Drug / Chemotherapeutic agent	Clinical usage	References	Limitations
Cisplatin, [Pt NH_1Cl_2] Cis–diamminedichloroplatinum(II)	Antitumor drug in clinical use against solid malignancies, ovarian, particularly testicular	[15]	Intrinsic and acquired resistance, systemic cytoxicity *viz.,* gastrointestinal, nephro, neurotoxicity
Oxaliplatin, [Pt(ox)(DACH)] DACH = R,R–1,2–diamminocyclohexane trans–L–1,2–diamminocyclohexaneoxalate platinum(II)	Metastatic cancers, ovarian and colorectal cancer	[16]	Mild hematologic and gastrointestinal side effects and peripheral neuropathy
Trinuclear Platinum compound (BBR 3464)	Human tumor types, Resistant to chemotherapy *viz.,* melanomas and gastric and lung carcinomas	[17]	Toxic effects comparable with those of cisplatin in terms of neurotoxicity and myelotoxicity
Imidazolium trans–[tetrachloro(dimethylsulphoxide) (imidazole)–ruthuenate(III)] (NAMI–A)	Phase I–II clinical trials very active against colon carcinomas and their metastases	[18]	Low cytoxicity *in vitro*, painful blister formation, renal toxicity
Indazolium trans–[tetrachlorobis(1H–indazole)ruthenueate(III) (KP1019)	Phase–II clinical trials, moderately cytotoxic tumors	[19]	The only major side effect in applicable doses was slightly affected erythropoiesis
[(η^6– fluorene)Ru(en)Cl]PF_6	Radiolabelled cytotoxic agent; Breast and non–small cell lung cancer cell lines. Toxicity toward prostate cancer cells lines	[20]	Over–radio exposure in organs like kidney and liver
Zn(II) complexes containing 4,4 dinonyl–2,2–bipyridine (bpy)and tropolones or 1–phenyl–1–methyl–4–R–5–pyrazolones	Selective activity towards cancer cells, being more active on DU145 and PC–3 cells with respect to LNCaP cells	[21]	Complete mechanism of action and the structure–cellular activity of this class of metal complexes not explained yet.

Table 2: Selected Crystallographic data for the complex **1**.

Parameter	
Empirical formula	$C_{48}H_{74}Cl_2N_{12}O_{12}Zn_2$
Formula weight (g mol^{-1})	1212.83
Crystal system	Triclinic
Space group	*P–1.*
a (Å)	12.0599 (7)
b (Å)	12.4700 (5)
c (Å)	21.057 (1)
α (deg)	80.753 (4)°
β (deg)	85.925 (4)°
γ (deg)	73.453 (4)°
V($Å^3$)	2995.0 (3)
Z	2
D_{calc} (Mg m^{-3})	1.345
μ (mm^{-1})	0.96
F(000)	1272
Crystal size (mm)	0.36 × 0.29 × 0.14
Temp (K)	100 (2)
Measured reflections	23434
Unique reflections	3526
θ range (deg)/ completeness (%)	2.6 to 27.00
No. of data/parameters/restraints	12452/650/4
GoF[a]	0.803
R^b[I>2σ (I)]	0.094
$wR_2{}^b$(all data)	0.288
Largest diff. peak/hole (e.$Å^{-3}$)	1.13/–0.61

[a]GoF is defined as $\{\Sigma[w(F_0^2-F_c^2)]/(n-P)\}^{1/2}$ where n is the number of data and p is the number of parameters. [b]$R = \{\Sigma||F_0|-|F_c||/\Sigma|F_0|$, $wR^2 = \{\Sigma\, w(F_0^2-F_c^2)^2 / \Sigma\, w(F_0^2)^2\}^{1/2}$.

Figures

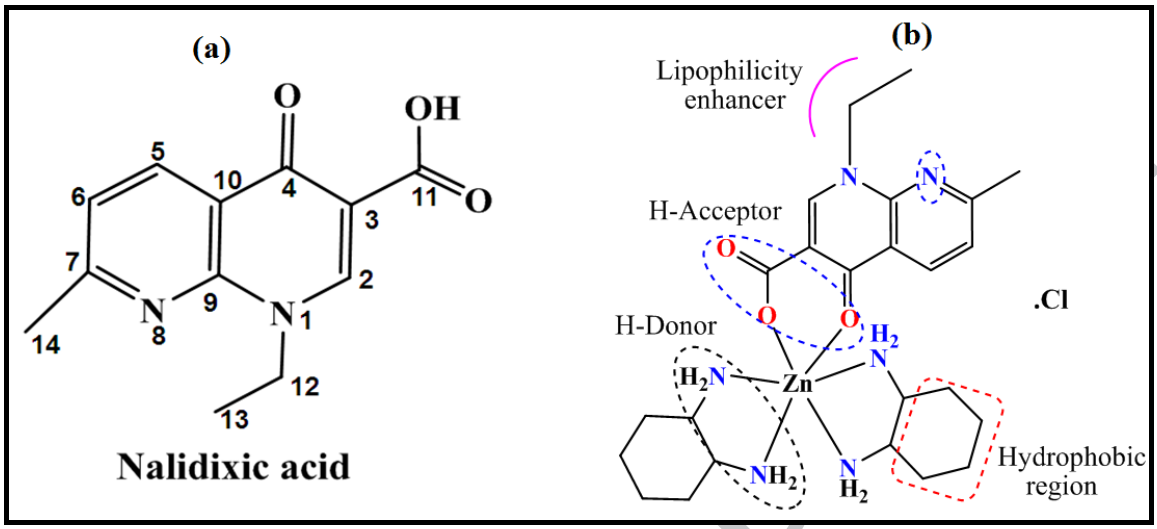

Fig. 1

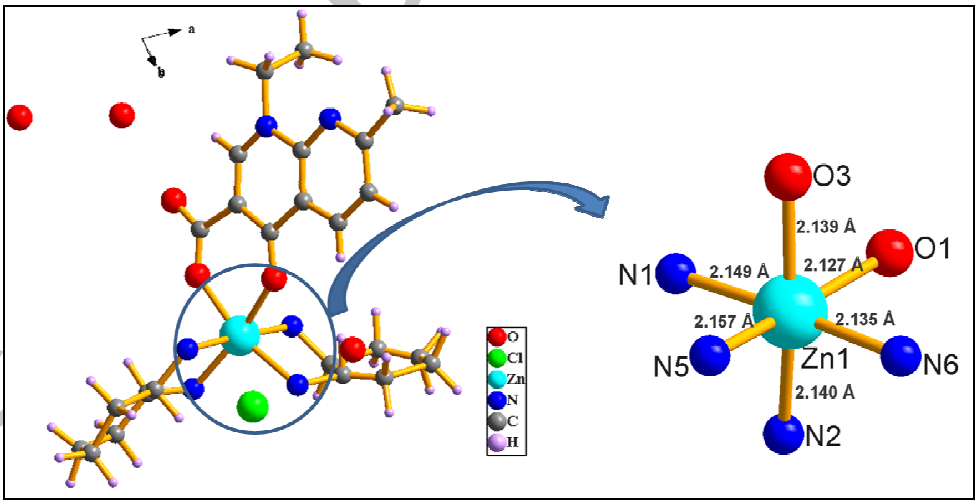

Fig. 2

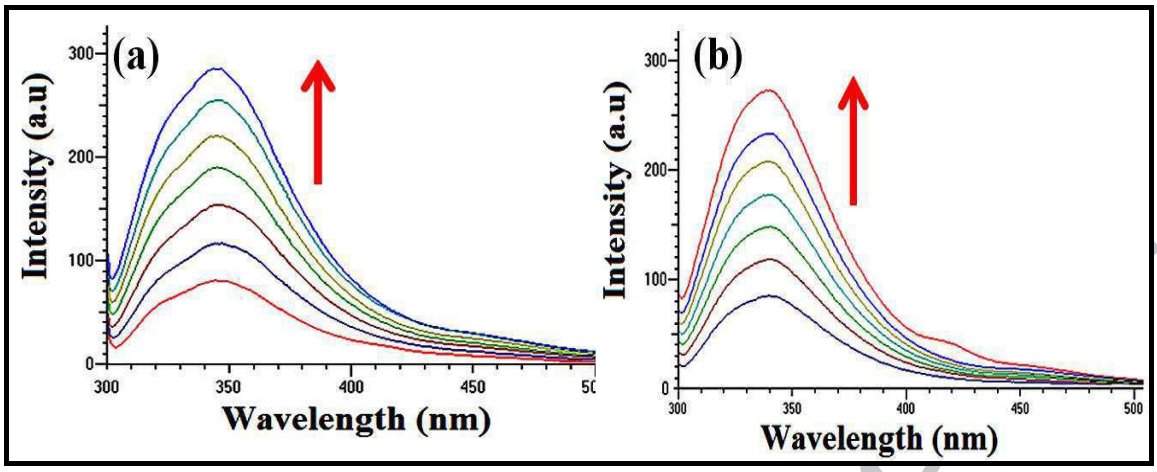
(a)
Intensity (a.u)
Wavelength (nm)
(b)
Intensity (a.u)
Wavelength (nm)

Fig. 3

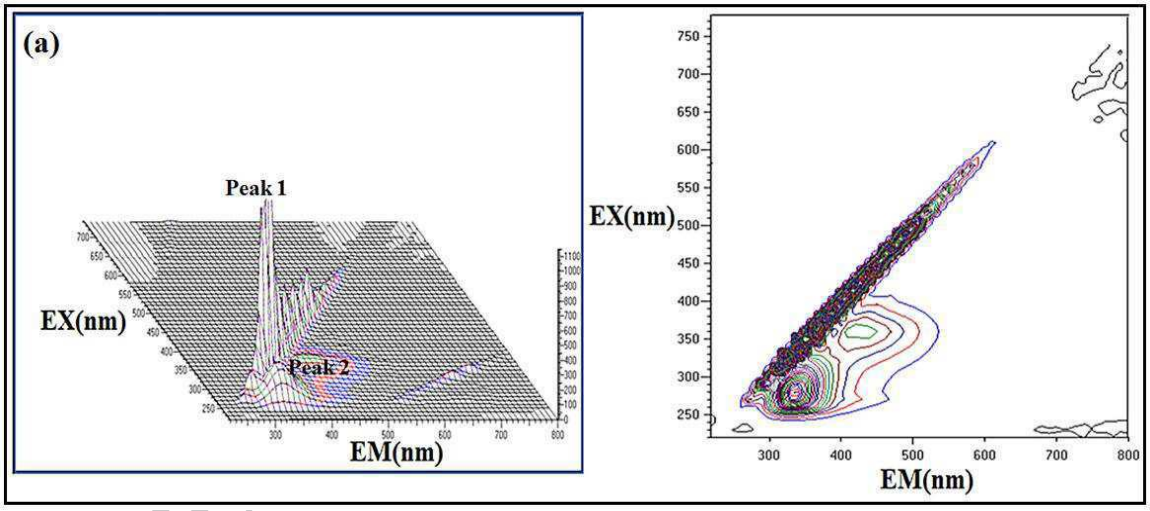
(a)
Peak 1
Peak 2
EX(nm)
EM(nm)
EX(nm)
EM(nm)

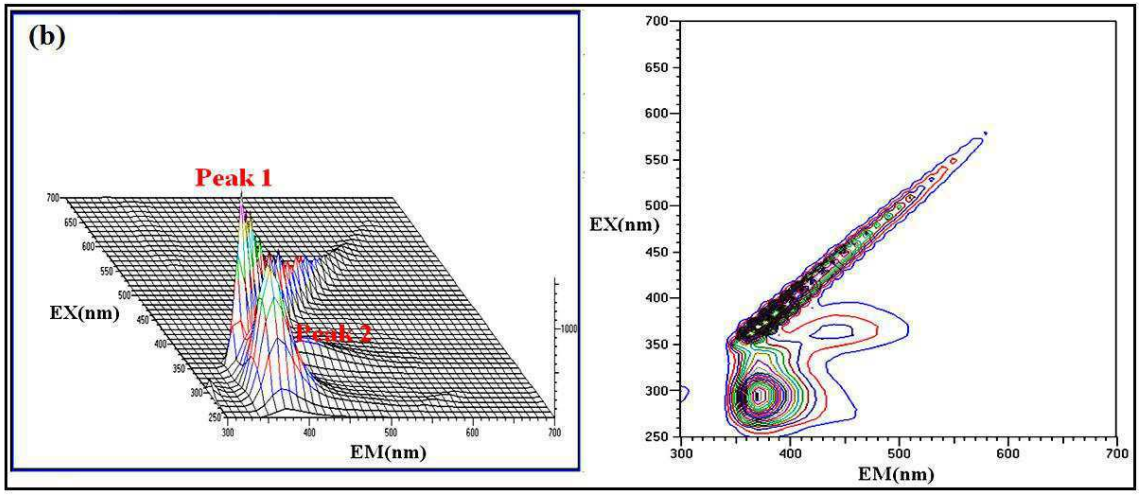
(b)
Peak 1
Peak 2
EX(nm)
EM(nm)
EX(nm)
EM(nm)

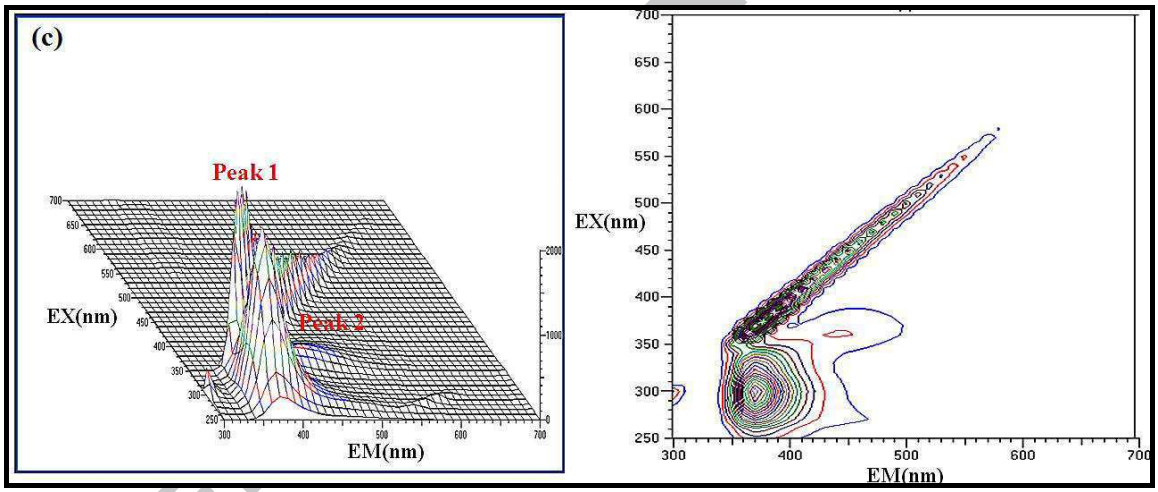
(c)
Peak 1
Peak 2
EX(nm)
EM(nm)
EX(nm)
EM(nm)

Fig. 4

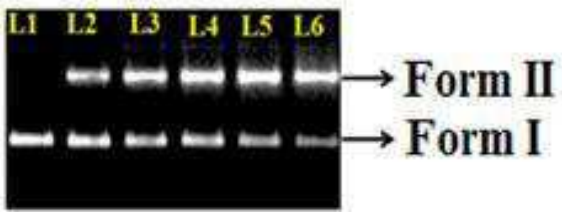
L1
L2
L3
L4
L5
L6
Form II
Form I

Fig. 5

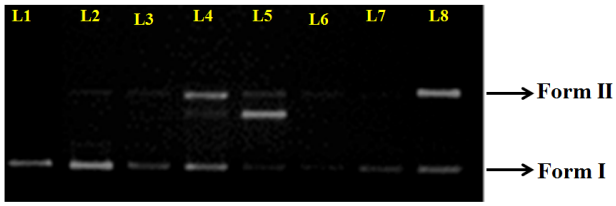

Fig. 6

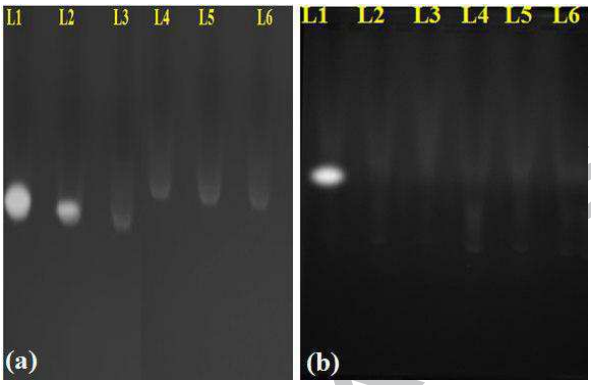

Fig. 7

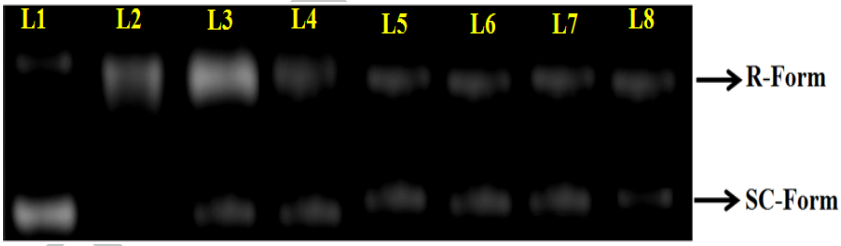

Fig. 8

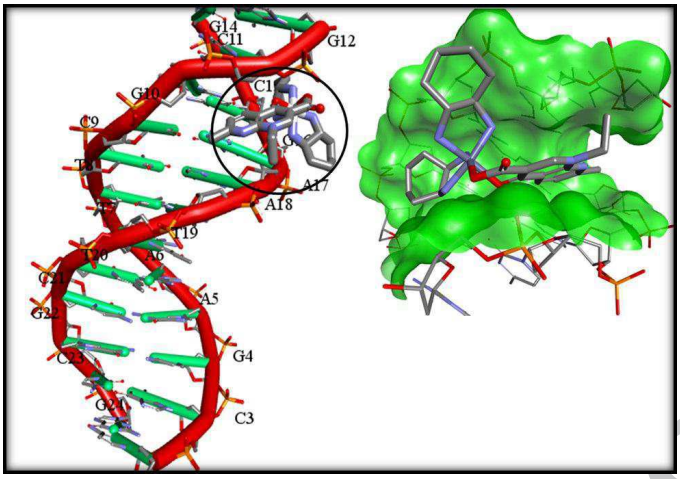
G14
C11
G12
G10
C9
A17
A18
T19
A6
A5
G22
G4
C3

Fig.9

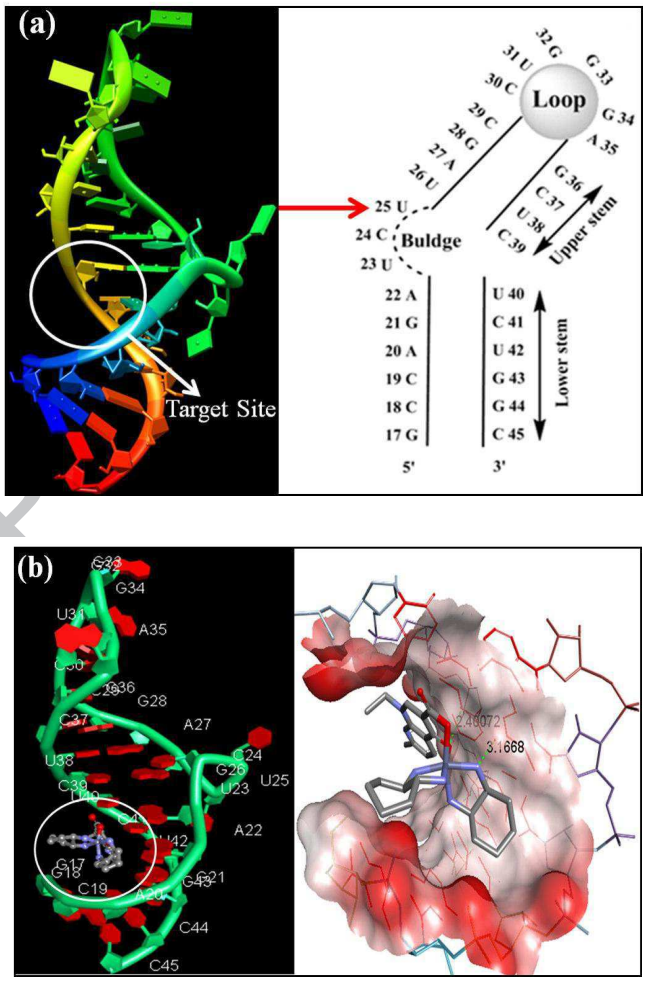
(a)
Target Site
Loop
Buldge
Upper stem
Lower stem
32 G
G 33
31 U
30 C
29 C
28 G
27 A
26 U
G 34
A 35
G 36
C 37
U 38
C 39
25 U
24 C
23 U
22 A
21 G
20 A
19 C
18 C
17 G
U 40
C 41
U 42
G 43
G 44
C 45
5'
3'
(b)
G34
U31
A35
G28
A27
C27
U38
C24
G26
U25
U23
A22
C19
C44
C45

Fig. 11

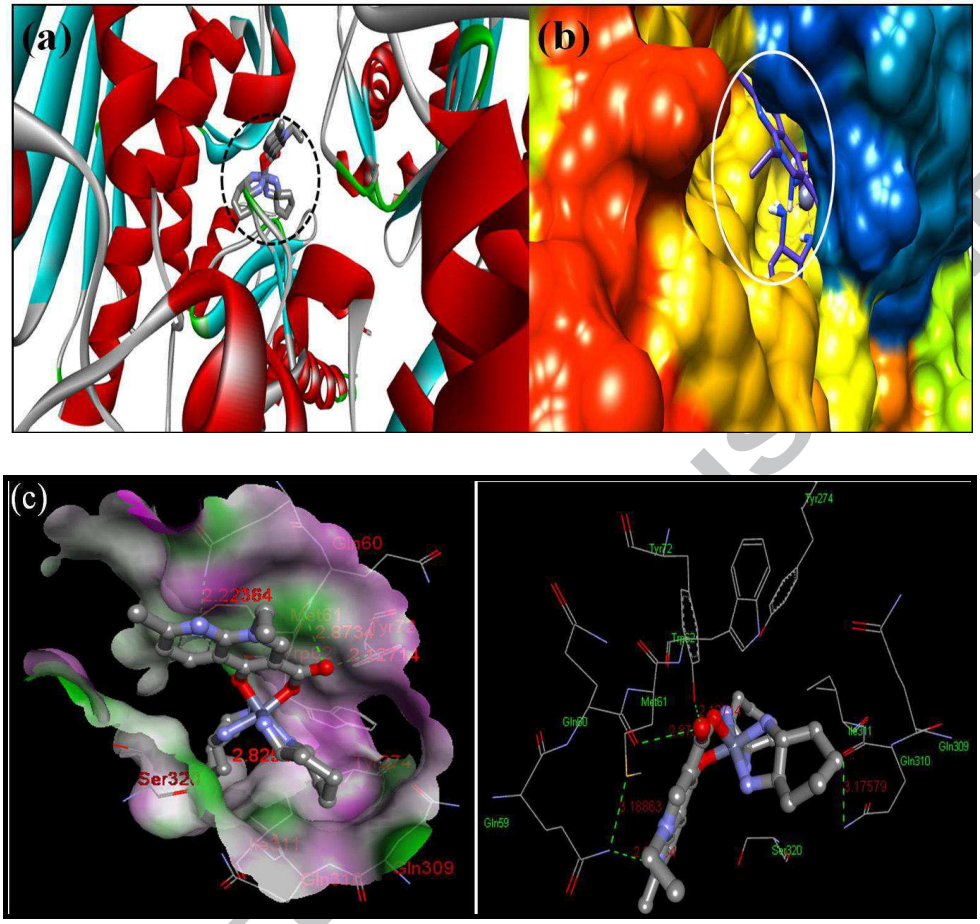
(a)
(b)
(c)
Gln60
2.22364
Met61
Ser32
Gln309
Tyr274
Tyr72
Trp2
Met61
Gln60
Ile311
Gln309
Gln310
Gln59
Ser320

Fig. 11

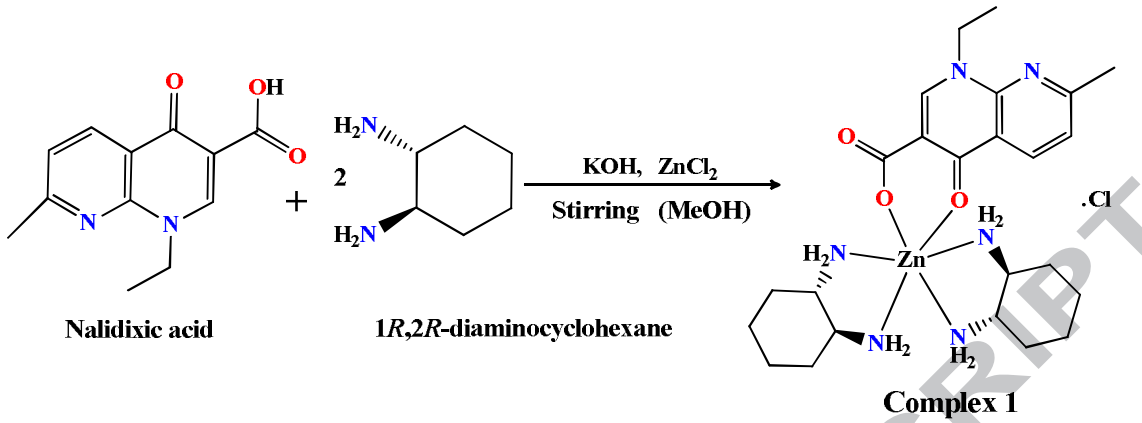

Scheme 1: Synthetic route for the complex **1**

Graphical Abstarct Synopsis

Molecular docked model of Zn(II) nalidixic acid–DACH complex, **1** targeting TAR RNA.

Graphical Abstarct Pictogram

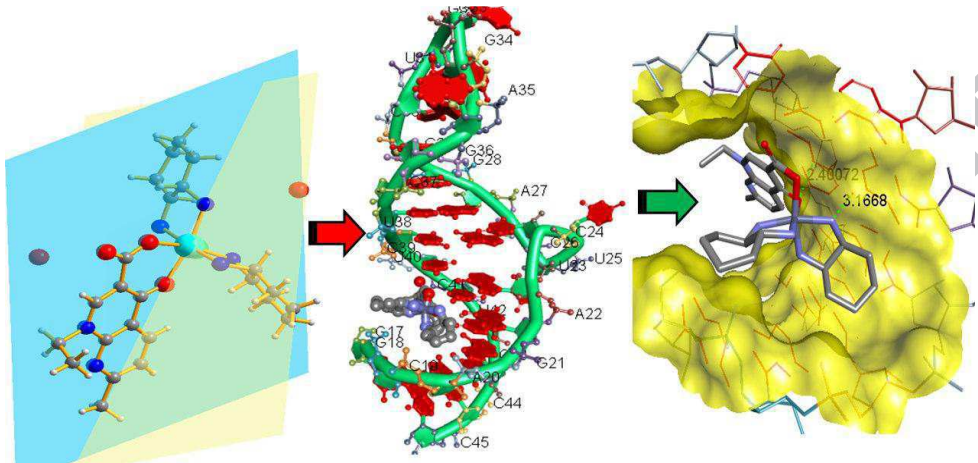

Complex 1 **Targeting TAR RNA**

Research Highlights

- Zinc(II) based drug entity, **1** was synthesized from nalidixic acid and DACH ligands.
- Complex **1** showed avid binding propensity for tRNA as compared to DNA.
- Complex **1** was found to be a catalytic inhibitor of human Topo–II.
- Hydrolytic cleavage of pbr322 DNA by complex 1 was validated by T4 DNA ligation assay.
- Molecular docking results corroborated well with other spectroscopic results.